

# Differential rotation and meridional flow in the solar convection zone and beneath

L.L. KITCHATINOV<sup>1,2</sup> and G. RÜDIGER<sup>1</sup>

<sup>1</sup> Astrophysikalisches Institut Potsdam, An der Sternwarte 16, 14482, Potsdam, Germany

<sup>2</sup> Institute for Solar-Terrestrial Physics, PO Box 4026, Irkutsk 664033, Russia

Received 30 April 2005; accepted 30 May 2005; published online 1 July 2005

**Abstract.** The influence of the basic rotation on anisotropic and inhomogeneous turbulence is discussed in the context of differential rotation theory. An improved representation for the original turbulence leads to a  $\Lambda$ -effect which complies with the results of 3D numerical simulations. The resulting rotation law and meridional flow agree well with both the surface observations ( $\partial\Omega/\partial r < 0$  and meridional flow towards the poles) and with the findings of helioseismology. The computed equatorward flow at the bottom of convection zone has an amplitude of about 10 m/s and may be significant for the solar dynamo. The depth of the meridional flow penetration into the radiative zone is proportional to  $\nu_{\text{core}}^{0.5}$ , where  $\nu_{\text{core}}$  is the viscosity beneath the convection zone. The penetration is very small if the tachocline is laminar.

**Key words:** Sun: rotation – stars: rotation – stars: activity

©0000 WILEY-VCH Verlag GmbH & Co. KGaA, Weinheim

## 1. Motivation

The internal solar rotation is well-known from helioseismology (Wilson et al. 1997; Kosovichev et al. 1997; Schou et al. 1998). The decrease of angular velocity with latitude observed on the solar surface survives throughout the convection zone. The differential rotation decreases sharply with depth in the thin ‘tachocline’ beneath the convection zone. The helioseismology inversions also show a considerable increase of rotation rate with depth just beneath the solar surface (Fig. 1).

The present paper demonstrates how mean-field models work to explain the overall pattern of the internal solar rotation and to derive the related meridional flow. To this end

- our former theory of angular momentum transport by rotating turbulence (Kitchatinov & Rüdiger 1993, hereafter KR93) is extended to the case of slow rotation
- the global stellar circulation model is modified to include the meridional flow penetration below the convection zone.

The currently debated penetration (Nandy & Choudhury 2002; Gilman & Miesch 2004) may be important for advection-dominated models of the solar dynamo (Choudhuri, Schüssler & Dikpati 1995; Dikpati & Gilman 2001; Bonanno et al. 2002). The dependence of the penetration depth

on basic parameters is computed with our global stellar circulation model. The new simulations include also a computation of the solar tachocline with one of the currently discussed tachocline models (Rüdiger & Kitchatinov 1997; MacGregor & Charbonneau 1999).

The angular momentum fluxes inside the convection zone basically depend on the Coriolis number,

$$\Omega^* = 2\tau_{\text{conv}}\Omega, \quad (1)$$

where  $\Omega$  is the angular velocity and  $\tau_{\text{conv}}$  is the convective turnover time. The numerical models (Kitchatinov & Rüdiger 1995, 1999; Küker & Stix 2001) based on the  $\Lambda$ -effect theory of KR93 had practically no free parameters but reproduced the main features of the solar rotation law and predicted correctly the trend of the surface differential rotation with stellar mass and rotation rate (see Hall 1991; Barnes et al. 2005).

The characteristic value of the Coriolis number for the Sun exceeds unity,  $\Omega_{\odot}^* \simeq 6$ , and it is even larger for rapidly rotating stars. The Coriolis number varies, however, with depth inside the Sun (cf. Fig. 2) and becomes rather small near the surface. The former models did not concern the near-surface region (e.g. Kitchatinov & Rüdiger 1995).

The present paper extends the former results by using a more general representation for the spectral tensor of turbulent convection. The resulting expressions for the  $\Lambda$ -effect include a free parameter which is unimportant for  $\Omega^* \gg 1$ . Its value can be restricted by numerical experiments. The new

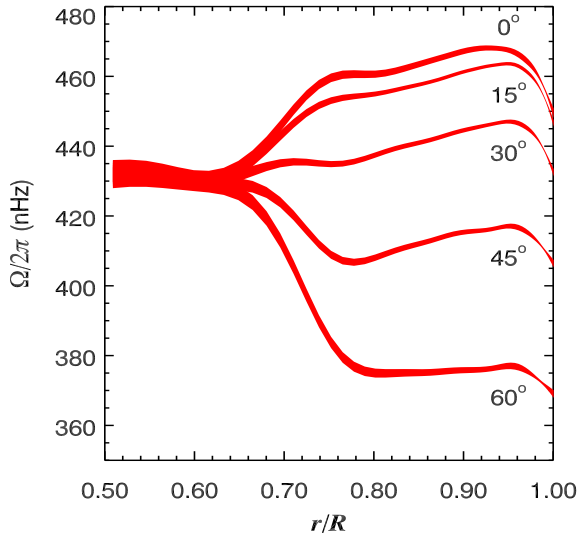


**Fig. 1.** Internal solar rotation from helioseismology. Courtesy NSF's National Solar Observatory. The numbers give the latitude rather than the colatitude.

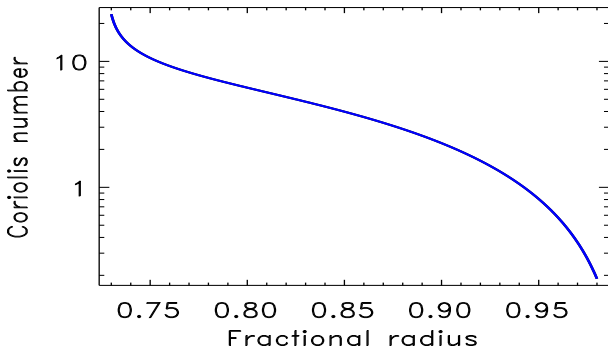


**Fig. 2.** Profile of the Coriolis number (1) in the solar model of Stix & Skaley (1990).

model shows agreement with both the observed rotation law and the meridional flow near the solar surface. It predicts the meridional flow towards equator with an amplitude of about 10 m/s at the bottom of the convection zone.

## 2. Angular momentum transport

### 2.1. Basic relations

The ability of turbulence to transport angular momentum is reflected in the structure of the correlation tensor,

$$Q_{ij} = \langle u'_i(\mathbf{x}, t) u'_j(\mathbf{x}, t) \rangle, \quad (2)$$

of the fluctuating velocity  $\mathbf{u}'$ . The radial and the latitudinal angular momentum fluxes are proportional to the off-diagonal components,  $Q_{r\phi}$ ,  $Q_{\theta\phi}$ , of the tensor in spherical coordinates. The fluxes are finite even for the case of rigid rotation; they are conventionally parameterized as

$$Q_{r\phi}^A = \nu_T \Omega V \sin \theta, \quad Q_{\theta\phi}^A = \nu_T \Omega H \cos \theta. \quad (3)$$

The eddy viscosity,  $\nu_T$ , is introduced here for dimensional reasons,  $V$  and  $H$  are the normalized vertical and horizontal fluxes.

Negative  $V$  also for slow rotation is required to explain the negative radial gradient of the angular velocity seen in the subsurface layer in Fig. 1. The equatorial acceleration, on the other hand, demands positive  $H$  (Rüdiger 1989). For a nonuniform rotation the correlation tensor (2) includes the diffusive part,  $Q^\nu$ , which is defined by the eddy viscosity tensor,  $\mathcal{N}_{ijkl}$ ,

$$Q_{ij} = Q_{ij}^A + Q_{ij}^\nu, \quad (4)$$

with

$$Q_{ij}^\nu = -\mathcal{N}_{ijkl} \frac{\partial \bar{u}_k}{\partial x_l}, \quad (5)$$

where  $\bar{\mathbf{u}}$  is the mean velocity.

### 2.2. 3D simulations

It is not easy to separate the  $A$ -effect from its viscous counterpart in the results of 3D numerical simulations. Käpylä et al. (2004) suggest that the diffusive momentum fluxes may be small in the box simulations. They are also reporting  $H > 0$ .

Already Pulkkinen et al. (1993) found that the function  $V$  is negative and  $H$  is positive. The results of Rieutord et al. (1994) confirmed the positive  $H$  but the vertical flux  $V$  was small. Chan (2001) found very clear results also with positive  $H$  but with negative  $V$ . The equatorial value of the latter proved to be rather small.

Simulations of compressible thermal convection under the influence of rotation were also made with the finite-difference, fractional-step code NIRVANA (version II) in a small rectangular box defined on a Cartesian grid (Ziegler 1998, 1999; Rüdiger et al. 2005b). The Coriolis number (1) varied from about unity at the top of the convection box to about four at its base. The results agree with those of Chan (2001) and Käpylä et al. (2004) in providing negative  $V$  and positive  $H$ . The horizontal flux is strongly concentrated towards the equator.

The box simulations can be summarized as follows. The radial flux  $V$  of the angular momentum is always negative. Its equatorial value vanishes for  $\Omega^* > 1$  in agreement with KR93 for fast rotation. The horizontal flux  $H$  is positive in all simulations. It vanishes at the poles as it should be from symmetry reasons.

### 2.3. Quasilinear theory

The quasilinear theory of the angular momentum transport by rotating turbulence in density-stratified fluids results in the expressions

$$V = V^{(0)}(\Omega^*) - H^{(1)}(\Omega^*) \cos^2 \theta, \\ H = H^{(1)}(\Omega^*) \sin^2 \theta, \quad (6)$$

for the normalized fluxes<sup>1</sup>. The coefficients  $V^{(0)}$  and  $H^{(1)}$ ,

$$V^{(0)} = \left( \frac{\ell_{\text{CORR}}}{H_\rho} \right)^2 (J_0(\Omega^*) + aI_0(\Omega^*)), \\ H^{(1)} = \left( \frac{\ell_{\text{CORR}}}{H_\rho} \right)^2 (J_1(\Omega^*) + aI_1(\Omega^*)), \quad (7)$$

<sup>1</sup> see the Appendix for more details

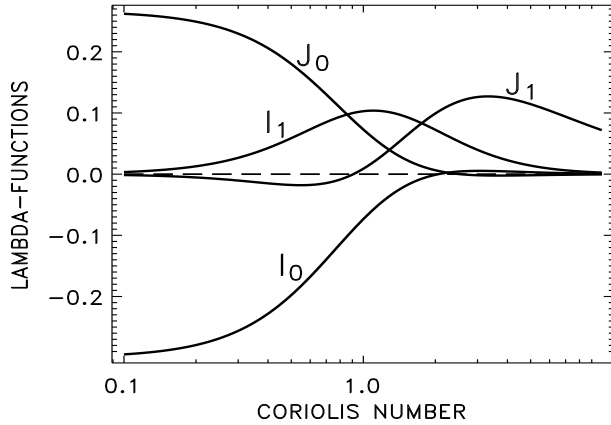


**Fig. 3.** The functions of the Eq. (7). Only  $J_0$  and  $I_0$  remain finite at small Coriolis numbers and they have opposite signs. For rapid rotation, i.e. large  $\Omega^*$ ,  $J_1$  dominates all other functions.

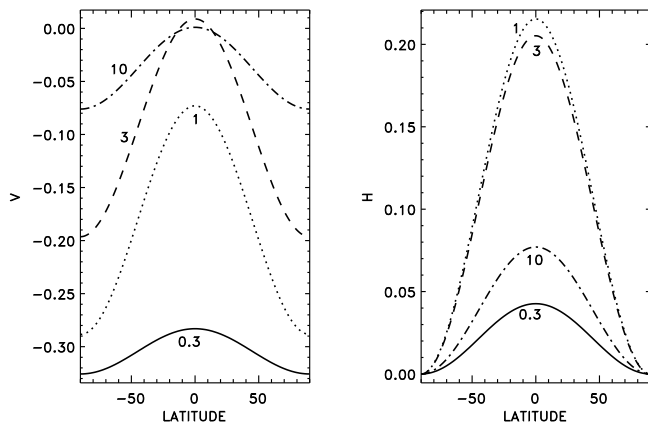


**Fig. 4.** Normalized fluxes of angular momentum (6) in dependence on latitude for  $a = 2$  and  $\Omega^*$  from 0.3 to 10. The lines are marked by the correspondent values of the Coriolis number  $\Omega^*$ .

depend on the Coriolis number via the functions  $J$  and  $I$  given by (A18) and (A19). The functions  $J_0$  and  $J_1$  are the same as in KR93. All these ‘ $\Lambda$ -functions’ are plotted on Fig. 3. It can be seen from the plots and Eq. (7) that a positive  $H^{(1)}$  requires a slightly positive anisotropy parameter  $a$  defined by (A12) and (A15). On the other hand, a negative  $V$  for slow rotation can be reproduced only with  $a > 1$ . The vanishing  $V$  at the equator for rapid rotation is due to the rapid decrease of the functions  $J_0$  and  $I_0$  with  $\Omega^*$ .

Figure 4 shows the normalized fluxes,  $V$  and  $H$ , as functions of latitude for  $a = 2$ , a value that was also used to model differential rotation and meridional flow as discussed below. The resulting profiles are in agreement with all the main findings of the box simulations, i.e.

- positive  $H$ ,
- increasingly negative  $V$  with increasing latitude,
- negative equatorial  $V$  approaching zero with increasing rotation rate.

The anisotropy relation

$$\langle u_\phi^2 \rangle - \langle u_r^2 \rangle = \frac{1}{8\rho^2} \frac{d^2}{dz^2} \left( (1 - 2a/5) \rho^2 \ell_{\text{corr}}^2 \langle u^2 \rangle \right) \quad (8)$$

follows from (A16) which for  $a = 0$  yields positive (negative) values in the upper (lower) part of the solar convection zone. With  $a \simeq 2$  the amplitude of this anisotropy is strongly reduced in the upper part of the convection zone. In its lower part, the effect is completely quenched by the rapid rotation and the turbulence there remains vertically-dominated.

### 3. The model

The global flow in the solar convection zone was computed with our former model (Kitchatinov & Rüdiger 1999) which now applies the new expressions (7) for the  $\Lambda$ -effect with the functions (A18) and (A19). The model solves the steady mean-field momentum equation,

$$(\bar{\mathbf{u}} \cdot \nabla) \bar{\mathbf{u}} + \frac{1}{\rho} \nabla \cdot (\rho \mathbf{Q}) + \frac{1}{\rho} \nabla P = \mathbf{g}, \quad (9)$$

for axisymmetric mean flow  $\bar{\mathbf{u}}$  simultaneously with the entropy equation

$$\rho T \bar{\mathbf{u}} \cdot \nabla S + \text{div} (\mathbf{F}^{\text{conv}} + \mathbf{F}^{\text{rad}}) = 0. \quad (10)$$

The entropy equation is needed to define the baroclinic part of the meridional flow as well as the eddy transport coefficients for the nonrotating case, e.g.,

$$\nu_T = - \frac{\tau_{\text{corr}} \ell_{\text{corr}}^2 g}{15 c_p} \frac{\partial S}{\partial r}. \quad (11)$$

The model accounts for the anisotropy and quenching of the eddy heat transport coefficients due to global rotation (see Rüdiger et al. 2005a, for details).

The usual stress-free and zero-penetration boundary conditions are applied. The lower boundary is located at the base of the convection zone (Model 1). In this model the boundary conditions exclude any penetration of meridional flow in the stably stratified layer beneath the convection zone. The magnetic tachocline model by Rüdiger & Kitchatinov (1997) is also used in Model 1 so that the rotation law is computed for the entire volume of the Sun. The model realizes the magnetic tachocline as a Hartmann layer due to a weak internal magnetic field of the solar radiative core. The tachocline modeling has no influence on the rotation law computed for the convection zone proper. It only uses the results of these computations as the top-boundary condition for the tachocline.

Penetration of the meridional flow into the stably stratified layer beneath the convection zone has been probed in former models but it was always weak. We now rediscuss this issue because the penetration became important in relation with new ideas of solar dynamo theory. The bottom boundary is thus placed beneath the convection zone inside the stably stratified region (Ekman layer model, Model 2). For numerical reasons, an extra but small isotropic and uniform viscosity and thermal conductivity were prescribed for the entire computation region. The code is flexible enough to apply a nonuniform grid with about 300 grid points beneath the convection zone to resolve even a shallow penetration. The dependence of the penetration depth,  $D_{\text{pen}}$ , on the prescribed effective viscosity ( $\nu_{\text{core}}$ ) is computed with Model 2. The computation of a tachocline makes little sense in combination with this model and it was not attempted.

With the thermal boundary conditions both spherically symmetric heating from below at the bottom of the computational domain and black-body radiation of the photosphere are introduced into the model. The top boundary of the model is placed shortly below the photosphere to exclude the surface layer with very sharp stratification for which case our representation for the  $\Lambda$ -effect is certainly incomplete. Nevertheless, in order to include the supergranulation layer into the simulations, the external boundary was shifted from its usual position at  $x_e = 0.95$  to  $x_e = 0.98$ .

Yet, the surface layers are now unstable to large-scale thermal convection with the usual value  $\ell_{\text{corr}}/H_p = 1.7$  of the mixing length  $\alpha_{\text{MLT}}$  (Tuominen et al. 1994). We had to increase the parameter to  $\alpha_{\text{MLT}} = 2.1$  to avoid this instability. With such a large value the mixing length is larger than the density scale height, which is problematic for the construction procedure of the spectral tensor used in the Appendix.

The solar model of Stix and Skaley (1990) is used. The temperature and density at the external boundary are  $\rho_e = 1.37 \cdot 10^{-3} \text{ g cm}^{-3}$  and  $T_e = 1.03 \cdot 10^5 \text{ K}$ , taken as the input parameters of the simulations.

## 4. Results and discussion

### 4.1. Global flow structure

After a confrontation of the quasilinear theory of the  $\Lambda$ -effect with the results of the numerical simulations only positive values of the anisotropy  $a$ -parameter are reasonable. We shall see that for  $a > 0$  the rotation law in the supergranulation layer well approaches the observed state with  $\partial\Omega/\partial r < 0$  shown in Fig. 1. The meridional flow at the surface is poleward and it is equatorward at the bottom of the convection zone. In particular, the resulting amplitude of the flow is an important outcome of the simulations. Doppler measurements by Komm et al. (1993) show a poleward flow on the surface, and the helioseismology indicates that this direction of the circulation persists to a depth of at least 12 Mm (Zhao & Kosovichev 2004). A characteristic amplitude for the surface velocity is 10 m/s.

The global circulation computed with  $a = 2$  is shown in the Figs. 5 and 6. The radial gradient of  $\Omega$  and the direction of meridional flow in the subsurface region are close to the observed state. The computed rotation law reflects all the known basic features, i.e.

- equatorial acceleration,
- negative gradients of  $\Omega$  in the outer region,
- small variation with depth for latitudes  $\sim 30^\circ$ ,
- shallow tachocline

(Fig. 5). The clear subrotation of the surface region ( $\partial\Omega/\partial x < 0$  for  $x > 0.9$ ) is mainly related to the radial fluxes of angular momentum. Figure 3 shows that the functions  $I_0$  and  $J_0$  responsible for the radial fluxes are almost completely quenched for  $\Omega^* > 2$ , which corresponds to  $x \leq 0.9$  (Fig. 2). Below this depth the results are thus uninfluenced by the special choice of  $a$ . The subsurface increase

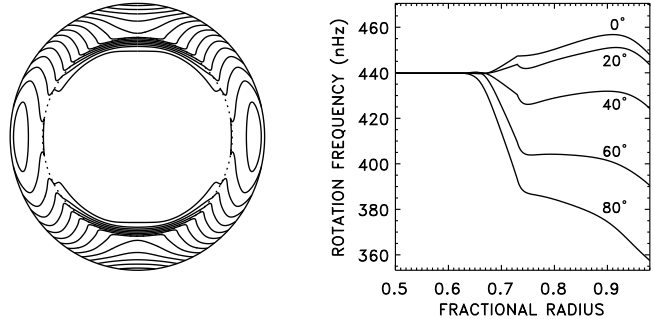


**Fig. 5.** Rotation law for  $a = 2$ . Left: angular velocity isolines. Right: depth profiles of the rotation rate.

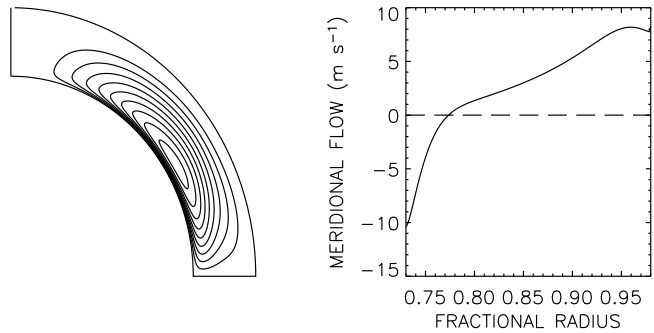


**Fig. 6.** Streamlines of the meridional flow (left) and flow velocity for  $45^\circ$  latitude as function of depth (right) for  $a = 2$ . Positive velocity means poleward flow. One cell of anticlockwise circulation occupies the entire convection zone.

of rotation rate may be important for the solar dynamo (Brandenburg 2005).

The meridional flow at the surface is poleward. Its amplitude is slightly below 10 m/s. The circulation consists of a single cell with a return equatorward flow at the bottom. The flow reversal occurs rather deep so that the amplitude of the bottom velocity,  $\sim 10$  m/s, is not small despite of the strong downward density increase.

The poles are warmer than the equator by 2.3 K in the model given in Figs. 5 and 6 for  $a = 2$ . Many computations with various  $a$ -values were made. The models with  $a \simeq 2$  reproduce the observations most closely.

Angular momentum transport by rotating turbulence is known to originate from anisotropies existing in the turbulence and/or from any inhomogeneity of the turbulent fluid. For fast rotation the  $\Lambda$ -effect produced by an inhomogeneity is much stronger compared to the effect of pure anisotropy. This is probably because the rotation can easily modify the anisotropies, but not the stratification. The modification of the spectral tensor introduced in this paper influences the anisotropy with consequences for the  $\Lambda$ -effect and the resulting rotation law close to the surface. By this modification the anisotropy parameter  $a$  enters the theory. The parameter is fixed using the results of 3D numerical box simulations. Global simulations have made considerable progress recently (Robinson & Chan 2001; Brun & Toomre 2002; Brun, Miesch & Toomre 2004) but seem to suffer still from the problem of resolution for the smaller scales.

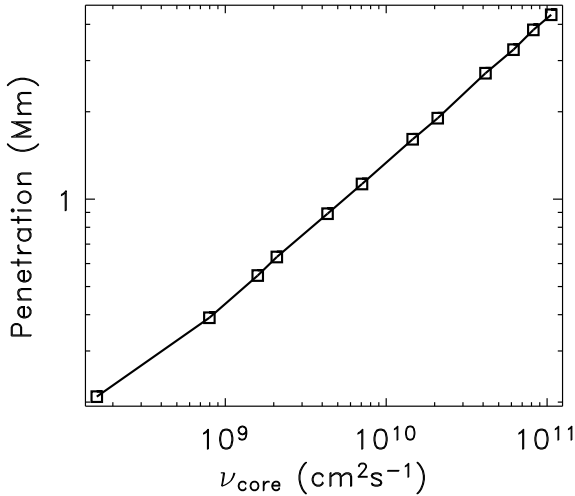


**Fig. 7.** Depth of penetration of the meridional flow into the radiative zone at latitude  $45^\circ$  in dependence on the viscosity prescribed for the convectively stable region. The computed dependence is very close to  $D_{\text{pen}} \propto \sqrt{\nu_{\text{core}}}$ .

#### 4.2. Penetration

With the Model 2 the penetration depth of the meridional circulation into the radiative zone was computed. The penetrating flow shows multiple reversals of the meridional velocity with increasing depth. The velocity amplitude decreases many times after each reversal. The penetration depth  $D_{\text{pen}}$  of Fig. 7 is defined as the distance from the base of the convection zone to the location of the first reversal of the sign of  $\bar{u}_\theta$ .

The slope in the plot of Fig. 7 is very close to 0.5. This result complies with the finding of Gilman & Miesch (2004) that the penetration under solar conditions belongs to the Ekman regime. The penetration of this type results from viscous drag imposed by the meridional flow at the base of the convection zone on the fluid below. The standard estimate for the Ekman depth is  $D_{\text{pen}} \sim \sqrt{\nu_{\text{core}}/2\Omega}$ . This is further supported by our finding that the variation of heat conductivity for constant  $\nu_{\text{core}}$  does not change  $D_{\text{pen}}$ . The computations, however, do not reproduce the expected dependence  $D_{\text{pen}} \propto \Omega^{-0.5}$ . The slope is not constant and slightly larger than -0.5. The rotation rate dependence is better (though still not precisely) reproduced by the relation,

$$D_{\text{pen}} \propto \left( \Omega^2 + \Omega \frac{\tan\theta}{2} \frac{d\Omega}{d\theta} \right)^{-1/4}, \quad (12)$$

expected for nonuniform rotation.

For large  $\nu_{\text{core}}$  the penetration has a considerable effect on the global circulation and the thermodynamics *inside* the convection zone. The meridional flow at the base of the convection zone is reduced and the differential rotation and the differential temperature are increased with allowance for penetration. This is in agreement with Rempel (2005) who found that the balance of the meridional forces in the tachocline region demands a latitudinal entropy gradient which then spreads into the convection zone by radial diffusion. The poles become even warmer with this effect and the pole-

equator temperature difference resulting from anisotropic diffusion inside the convection zone (Rüdiger et al. 2005a) is amplified. Our computations, however, show that the influence of the region of stable stratification on the global flow in the convection zone reduces with decreasing  $\nu_{\text{core}}$  and  $\chi_{\text{core}}^2$ . For the smallest  $\nu_{\text{core}}$  given in Fig. 7 the differential rotation and the temperature distribution inside the convection zone are almost the same as in models without penetration.

Our computations do not support any significant penetration of the meridional circulation beneath the convection zone. The calculations confirm our former result (Kitchatinov & Rüdiger 1995) that the penetration is very small unless the tachocline below the convection zone is strongly turbulent.

*Acknowledgements.* We wish to thank Axel Brandenburg for constructive comments. L.L.K. is grateful to the Alexander von Humboldt Foundation and to the Astrophysical Institute Potsdam for hospitality and the visitor support. Russian Foundation for Basic Research is also acknowledged (project 05-02-16326).

#### References

- Barnes, J.R., Cameron, A.C., Donati, J.-F., James, D.J., Marsden, S.C., Petit, P.: 2005, MNRAS 357, L1
- Bonanno, A., Elstner, D., Rüdiger, G., Belvedere, G.: 2002, A&A 390, 673
- Brandenburg, A.: 2005, ApJ 625, 539
- Brun, A.S., Toomre, J.: 2002, ApJ 570, 865
- Brun, A.S., Miesch, M.S., Toomre, J.: 2004, ApJ 614, 1073
- Chan, K.L.: 2001, ApJ 548, 1102
- Choudhuri, A.R., Schüssler, M., Dikpati, M.: 1995, A&A 303, L29
- Dikpati, M., Gilman, P.A.: 2001, ApJ 559, 428
- Gilman, P.A., Miesch, M.S.: 2004, ApJ 611, 568
- Hall, D.S.: 1991, in: I. Tuominen et al. (eds.), *The Sun and Cool stars*, Springer, Berlin, p. 353
- Käpylä, P.J., Korpi, M.J., Tuominen, I.: 2004, A&A 422, 793
- Kitchatinov, L.L.: 1987, GApFD 38, 273
- Kitchatinov, L.L., Rüdiger, G.: 1993, A&A 276, 96 (KR93)
- Kitchatinov, L.L., Rüdiger, G.: 1995, A&A 299, 446
- Kitchatinov, L.L., Rüdiger, G.: 1999, A&A 344, 911
- Komm, R.W., Howard, R.F., Harvey, J.W.: 1993, SoPh 147, 207
- Kosovichev, A.G., Schou, J., Scherrer, P.H.: 1997, SoPh 170, 43
- Küker, M., Stix, M.: 2001, A&A 366, 668
- MacGregor, K.B., Charbonneau, P.: 1999, ApJ 519, 911
- Nandy, D., Choudhuri, A.R.: 2002, Sci 296, 1671
- Pulkkinen, P., Tuominen, I., Brandenburg, A., Nordlund, A., Stein, R.F.: 1993, A&A 267, 265
- Rempel, M.: 2005, ApJ 622, 1320
- Rieutord, M., Brandenburg, A., Mangeney, A., Drossart, P.: 1994, A&A 286, 471
- Roberts, P.H., Soward, A.M.: 1975, AN 296, 49
- Robinson, F.J., Chan, K.L.: 2001, MNRAS 321, 732
- Rüdiger, G.: 1989, *Differential Rotation and Stellar Convection*, Gordon & Breach, New York
- Rüdiger, G., Kitchatinov, L.L.: 1997, AN 318, 273
- Rüdiger, G., Egorov, P., Kitchatinov, L.L., Küker, M.: 2005a, A&A 431, 345
- Rüdiger, G., Egorov, P., Ziegler, U.: 2005b, AN 326, 315
- Schou, J., Antia, H.M., Basu, S., et al.: 1998, ApJ 505, 390
- Stix, M., Skaley, D.: 1990, A&A 232, 234
- Tuominen, I., Brandenburg, A., Moss, D., Rieutord, M.: 1994, A&A 284, 259

<sup>2</sup> Prandtl number  $\nu_{\text{core}}/\chi_{\text{core}} = 1/8$  in our computations

Wilson, P.R., Burtonclay, D., Li, Y.: 1997, ApJ 489, 395  
 Zhao, J., Kosovichev, A.G.: 2004, ApJ 603, 776  
 Ziegler, U.: 1998, CoPhC 109, 111  
 Ziegler, U.: 1999, CoPhC 116, 65

## Appendix A: $\Lambda$ -effect by rotating inhomogeneous turbulence

Here we systematically derive the  $\Lambda$ -effect effect for anelastic turbulent flow of a rotating stratified fluid. The usual strategy to deal with rotating turbulence is to prescribe the turbulence of the nonrotating fluid and then to derive the influence of rotation on the given 'original' turbulence. Here a nonrotating anelastic flow,  $\text{div}(\rho\mathbf{u}) = 0$ , is considered.

The density stratification is basic for the existence of the  $\Lambda$ -effect. Fourier modes of the momentum density,

$$\hat{\mathbf{m}}(\mathbf{z}, \omega) = \int \exp(-i\mathbf{x} \cdot \mathbf{z} + i\omega t) \cdot \mathbf{m}(\mathbf{x}, t) \, d\mathbf{x} \, dt / (2\pi)^4, \quad (\text{A1})$$

are used in order to construct the spectral tensor,

$$\hat{M}_{ij}(\mathbf{z}, \mathbf{z}', \omega, \omega') = \langle \hat{m}_i(\mathbf{z}, \omega) \hat{m}_j(\mathbf{z}', \omega') \rangle, \quad (\text{A2})$$

of the fluctuating momentum density,  $\mathbf{m} = \rho\mathbf{u}$ . The turbulence is assumed statistically steady. The two new wave vectors,

$$\mathbf{k} = (\mathbf{z} - \mathbf{z}')/2, \quad \boldsymbol{\kappa} = \mathbf{z} + \mathbf{z}', \quad (\text{A3})$$

are introduced. Then

$$\hat{M}_{ij}(\mathbf{z}, \mathbf{z}', \omega, \omega') = \delta(\omega' + \omega) \hat{M}_{ij}^{(0)}(\boldsymbol{\kappa}, \mathbf{k}, \omega). \quad (\text{A4})$$

The dependence on  $\mathbf{k}$  describes the properties of the correlations on the small scale while the dependence on  $\boldsymbol{\kappa}$  accounts for the turbulence inhomogeneity on large scale (Roberts & Soward 1975). We further assume that the (nonhelical) turbulence does not possess any preferred directions other than its intensity gradient. The overall structure of the tensor,

$$\begin{aligned} \hat{M}_{ij}^{(0)} &= a\delta_{ij} + b\frac{k_i k_j}{k^2} + c\frac{1}{k^2}(\kappa_i k_j - \kappa_j k_i) + d\frac{\kappa_i \kappa_j}{k^2} \\ &+ e\frac{(\mathbf{k} \cdot \boldsymbol{\kappa})}{k^4}(\kappa_i k_j + \kappa_j k_i), \end{aligned} \quad (\text{A5})$$

differs from a former derivation (Kitchatinov 1987) by the last extra term. The symmetry condition  $\hat{M}_{ij}^{(0)}(\boldsymbol{\kappa}, \mathbf{k}, \omega) = \hat{M}_{ji}^{(0)}(\boldsymbol{\kappa}, -\mathbf{k}, \omega)$ , is fulfilled. The divergence-free conditions

$$\begin{aligned} (k_i + \kappa_i/2) \hat{M}_{ij}^{(0)} &= 0, \\ (k_j - \kappa_j/2) \hat{M}_{ij}^{(0)} &= 0, \end{aligned} \quad (\text{A6})$$

lead to two vector equations with two nontrivial components each, hence

$$\begin{aligned} a + b + c\frac{\kappa^2}{2k^2} + e\frac{(\mathbf{k} \cdot \boldsymbol{\kappa})^2}{k^4} &= 0, \\ a - 2c + d\frac{\kappa^2}{k^2} + e\frac{(\mathbf{k} \cdot \boldsymbol{\kappa})^2}{k^4} &= 0, \\ b + 2c + e\frac{\kappa^2}{k^2} &= 0, \\ c - 2d - 2e &= 0. \end{aligned} \quad (\text{A7})$$

The system is of rank 3 so that three unknowns can be expressed in terms of the other two (say)  $c$  and  $e$ . It is convenient to express  $c$  and  $e$  in terms of the spectra  $\hat{E}$  and  $\hat{E}_1$ , i.e.

$$\begin{aligned} c &= \frac{\hat{E}(\boldsymbol{\kappa}, k, \omega) - \hat{E}_1(\boldsymbol{\kappa}, k, \omega) \left( \frac{\kappa^2}{2k^2} - \frac{(\mathbf{k} \cdot \boldsymbol{\kappa})^2}{2k^4} \right)}{32\pi k^2 \left( 1 - \frac{\kappa^2}{4k^2} \right)}, \\ e &= \frac{\hat{E}_1(\boldsymbol{\kappa}, k, \omega)}{16\pi k^2}. \end{aligned} \quad (\text{A8})$$

This leads to

$$\begin{aligned} \hat{M}_{ij}^{(0)} &= \frac{\hat{E} - \hat{E}_1 \left( \frac{\kappa^2}{2k^2} - \frac{(\mathbf{k} \cdot \boldsymbol{\kappa})^2}{2k^4} \right)}{16\pi k^2 \left( 1 - \frac{\kappa^2}{4k^2} \right)} \times \\ &\times \left( \left( 1 - \frac{\kappa^2}{4k^2} \right) \delta_{ij} - \frac{k_i k_j}{k^2} + \right. \\ &+ \frac{1}{2k^2} (\kappa_i k_j - \kappa_j k_i) + \frac{\kappa_i \kappa_j}{4k^2} \left. \right) + \\ &+ \frac{\hat{E}_1}{16\pi k^2} \left( \frac{\kappa^2}{k^2} \left( \delta_{ij} - \frac{k_i k_j}{k^2} \right) - \frac{(\mathbf{k} \cdot \boldsymbol{\kappa})^2}{k^4} \delta_{ij} + \right. \\ &+ \left. \frac{(\mathbf{k} \cdot \boldsymbol{\kappa})}{k^4} (\kappa_i k_j + \kappa_j k_i) - \frac{\kappa_i \kappa_j}{k^2} \right). \end{aligned} \quad (\text{A9})$$

It is further assumed that  $\hat{E}$  and  $\hat{E}_1$  depend on the wave number  $k$  only rather than on the wave vector  $\mathbf{k}$ . The function  $\hat{E}$  is the spectrum of turbulence intensity,

$$\langle m^2(\mathbf{x}) \rangle = \rho^2 \langle u^2 \rangle = \int_0^\infty \int_0^\infty E(\mathbf{x}, k, \omega) \, dk \, d\omega, \quad (\text{A10})$$

with

$$E(\mathbf{x}, k, \omega) = \int \exp(i\mathbf{x} \cdot \boldsymbol{\kappa}) \hat{E}(\boldsymbol{\kappa}, k, \omega) \, d\boldsymbol{\kappa}. \quad (\text{A11})$$

The spectrum  $E_1$  does not contribute to the turbulence intensity but it controls the anisotropy,  $\langle u_r^2 \rangle / \langle u_\theta^2 \rangle$ . The dimensionless anisotropy parameter,  $a$ , can be written as

$$a = \frac{4}{\langle m^2(\mathbf{x}) \rangle} \int_0^\infty \int_0^\infty E_1(\mathbf{x}, k, \omega) \, dk \, d\omega, \quad (\text{A12})$$

and it can depend on position. For the special case of

- $\hat{E}_1/\hat{E} = \text{const} = a/4$ ,
- $E \propto \delta(k - \ell_{\text{corr}}^{-1})$  (mixing-length approximation),
- $\nabla \langle m^2 \rangle = -2\mathbf{g} \langle m^2 \rangle / L$  ( $\mathbf{g}$  is radial unit vector and  $L$  is a constant length),

the spectral tensor (A9) can be integrated over wave space to give the one-point correlation tensor, i.e.

$$\begin{aligned} Q_{ij} &= \frac{\langle u^2 \rangle}{1 + \ell_{\text{corr}}^2/L^2} \left( \frac{1}{3} \delta_{ij} + \frac{\ell_{\text{corr}}^2}{2L^2} (\delta_{ij} - g_i g_j) \right), \\ &- \frac{a \langle u^2 \rangle}{1 + \ell_{\text{corr}}^2/L^2} \frac{\ell_{\text{corr}}^2}{L^2} \frac{1}{15} (\delta_{ij} - 3g_i g_j). \end{aligned} \quad (\text{A13})$$

For the rms intensities in the radial and the horizontal directions it yields

$$\begin{aligned} \langle u_r^2 \rangle &= \frac{\langle u^2 \rangle}{1 + \ell_{\text{corr}}^2/L^2} \frac{1}{3} \left( 1 + \frac{\ell_{\text{corr}}^2}{L^2} \frac{2a}{5} \right), \\ \langle u_\theta^2 \rangle &= \langle u_\phi^2 \rangle = \frac{\langle u^2 \rangle}{1 + \ell_{\text{corr}}^2/L^2} \frac{1}{3} \left( 1 + \frac{3\ell_{\text{corr}}^2}{2L^2} - \frac{\ell_{\text{corr}}^2}{L^2} \frac{a}{5} \right). \end{aligned} \quad (\text{A14})$$

The condition that the turbulence intensities (A15) are positive-definite restricts the value of the anisotropy parameter  $a$ ,

$$-\frac{5L^2}{2\ell_{\text{corr}}^2} \leq a \leq \frac{15}{2} + \frac{5L^2}{\ell_{\text{corr}}^2}. \quad (\text{A15})$$

Isotropy ( $\langle u_r^2 \rangle = \langle u_\theta^2 \rangle$ ) results for  $a = 5/2$ . Although the turbulence is isotropic in this case, the rotation produces a  $\Lambda$ -effect with negative  $Q_{r\phi}$ .

The ratio  $\kappa/k$  in Eq. (A9) is of order of  $\ell_{\text{corr}}/L$ . For a weakly inhomogeneous turbulence, therefore, the terms of higher than second order in the scale ratio can be neglected so that

$$\begin{aligned} \hat{M}_{ij}^{(0)} &= \frac{\hat{E}(\boldsymbol{\kappa}, k, \omega)}{16\pi k^2} \left( \delta_{ij} - \left(1 + \frac{\kappa^2}{4k^2}\right) \frac{k_i k_j}{k^2} \right. \\ &+ \frac{1}{2k^2} (\kappa_i k_j - \kappa_j k_i) + \frac{\kappa_i \kappa_j}{4k^2} \Big) \\ &+ \frac{\hat{E}_1(\boldsymbol{\kappa}, k, \omega)}{16\pi k^4} \left( \frac{(\mathbf{k} \cdot \boldsymbol{\kappa})}{k^2} (\kappa_i k_j + \kappa_j k_i) - \frac{(\mathbf{k} \cdot \boldsymbol{\kappa})^2}{k^2} \delta_{ij} \right. \\ &\left. - \kappa_i \kappa_j + \frac{1}{2} \left( \kappa^2 + \frac{(\mathbf{k} \cdot \boldsymbol{\kappa})^2}{k^2} \right) (\delta_{ij} - k_i k_j / k^2) \right) \end{aligned} \quad (\text{A16})$$

results. This equation directly leads to the  $\Lambda$ -effect. After the standard derivations (KR93), one arrives at

$$\begin{aligned} Q_{ij}^A &= \nu_T \Omega_k g_l \left( V^{(0)}(\Omega^*) (g_i \epsilon_{jkl} + g_j \epsilon_{ikl}) \right. \\ &\left. - H^{(1)}(\Omega^*) \frac{(\mathbf{g} \cdot \boldsymbol{\Omega})}{\Omega^2} (\Omega_i \epsilon_{jkl} + \Omega_j \epsilon_{ikl}) \right). \end{aligned} \quad (\text{A17})$$

The azimuthal components of this tensor reproduce Eq. (3) with the normalized fluxes of angular momentum defined by (6) and (7). The functions  $J_0$  and  $J_1$  (7) are the same as in KR93,

$$\begin{aligned} J_0(\Omega^*) &= \frac{1}{2\Omega^{*4}} \left( 9 - \frac{2\Omega^{*2}}{1 + \Omega^{*2}} - \frac{\Omega^{*2} + 9}{\Omega^*} \arctan \Omega^* \right), \\ J_1(\Omega^*) &= \frac{1}{2\Omega^{*4}} \left( 45 + \Omega^{*2} - \frac{4\Omega^{*2}}{1 + \Omega^{*2}} \right. \\ &\left. + \frac{\Omega^{*4} - 12\Omega^{*2} - 45}{\Omega^*} \arctan \Omega^* \right), \end{aligned} \quad (\text{A18})$$

and the expressions

$$\begin{aligned} I_0(\Omega^*) &= \frac{1}{4\Omega^{*4}} \\ &\times \left( -19 - \frac{5}{1 + \Omega^{*2}} + \frac{3\Omega^{*2} + 24}{\Omega^*} \arctan \Omega^* \right), \\ I_1(\Omega^*) &= \frac{3}{4\Omega^{*4}} \\ &\times \left( -15 + \frac{2\Omega^{*2}}{1 + \Omega^{*2}} + \frac{3\Omega^{*2} + 15}{\Omega^*} \arctan \Omega^* \right) \end{aligned} \quad (\text{A19})$$

are new. For slow rotation ( $\Omega^* \ll 1$ ) only the radial flux of angular momentum exists, i.e.

$$J_0 \simeq \frac{4}{15}, \quad I_0 \simeq -\frac{3}{10}, \quad J_1 \simeq I_1 \simeq O(\Omega^{*2}). \quad (\text{A20})$$

Note that  $I_0$  is negative for slow rotation. For fast rotation ( $\Omega^* \gg 1$ ),  $J_1$  dominates all other functions,

$$J_1 \simeq \frac{\pi}{4\Omega^*}, \quad J_0 \simeq I_0 \simeq I_1 \simeq O(\Omega^{*-3}). \quad (\text{A21})$$

The contribution of the anisotropy parameter  $a$  vanishes for fast rotation.